

# Co-iterative augmented Hessian method for orbital optimization

Qiming Sun<sup>1</sup>

*Division of Chemistry and Chemical Engineering, California Institute of Technology, Pasadena, California 91125, USA<sup>a)</sup>*

Orbital optimization procedure is widely called in electronic structure simulation. We developed a second order orbital optimization algorithm co-iteration augmented Hessian (CIAH) method to search the orbital optimization solution. In this algorithm, the orbital optimization is embedded in the diagonalization procedure of the augmented Hessian (AH) equation. Approximations to Hessian matrix can be easily applied in this method to reduce the computational costs. We numerically tested the CIAH algorithm with the SCF convergence problem and the Boys localization. We found that CIAH algorithm has better SCF convergence and less computational costs than direct inversion iterative subspace (DIIS) algorithm. The numerical tests suggest that CIAH is a stable, reliable and efficient algorithm for orbital optimization problem.

## I. INTRODUCTION

Self-consistency field (SCF) is the cornerstone of electronic structure simulation. It is required as a start point by almost all electronic structure calculations. However, converging SCF to a reasonable solution is not a trivial problem. Direct inversion iterative subspace<sup>1,2</sup> (DIIS) was the most successful method to accelerate the SCF convergence. It was widely used in quantum chemistry program as the default optimization algorithm for SCF problem.

Convergence problems are often observed for DIIS algorithm when the system has open shell character or small HOMO-LUMO gap. In the past, many SCF optimization techniques such as damping,<sup>3</sup> level shift<sup>4</sup> and enhanced DIIS algorithms EDIIS,<sup>5</sup> ADIIS<sup>6</sup> were proposed to improve the DIIS convergence.<sup>7-14</sup> Although these techniques improved DIIS convergence performance, DIIS and the improved algorithms have three main issues: (i) As an error-vector based minimization method, DIIS algorithm does not guarantee the SCF solution being the true minimum. It is easy to have DIIS solution stuck at saddle point; (ii) DIIS algorithm does not honor the initial guess well. The optimization procedure may lead the wavefunction anywhere in the variational space; (iii) DIIS algorithm does not have effective options to control the optimization procedure. Although DIIS convergence procedure can be controlled by tuning the damping, level shift, subspace size, extrapolation/interpolation constraints and other advanced techniques,<sup>5-14</sup> the influence are unpredictable.

The issues of DIIS algorithm can be surmounted in the second order SCF optimization algorithm.<sup>15,16</sup> Second order algorithm (Newton or quasi-Newton methods) directly minimizes the function gradients with the assistance of Hessian matrix. The Hessian matrix can provide an optimal displacement in the parameter space and a judgement whether a solution is at saddle point or local minimum. By tuning step size and trust region, one can easily control the optimization procedure and constrain the solution to certain region.

In Newton's methods, explicitly constructing the Hessian matrix and its inverse matrix often leads to high computational cost. Quasi-Newton methods address the cost problem

by approximating the Hessian matrix (or its inverse) based on the change of gradients during the optimization. Such Hessian approximation may be a native choice for complicated object function. This is not an optimal scheme for SCF problem because the simple structure of SCF Hessian matrix is not recognized by the gradients-oriented quasi-Newton methods. It is not necessary to estimate the Hessian based on the updates of gradients. Stripping Hessian evaluation from gradients construction, one would gain larger flexibility to approximate the Hessian matrix. Since Hessian matrix serves mainly as an auxiliary metric to adjust the descending direction of the displacement, the accuracy of Hessian matrix is not critical to convergence procedure. Therefore, many physical significant considerations rather than pure numerical treatment can be brought into the Hessian approximation.

A practical problem for Newton's method is the treatment of the negative eigenvalue and the singularity of the Hessian matrix. Negative Hessian is common when system is out of the quadratic region. Non-invertible Hessian matrix is also regularly found near the saddle point. These problems may result in wrong direction or singular displacement in the parameter space. Level shift for Hessian is often used to fix the singularity problem and adjust the descending direction. Here, the augmented Hessian (AH) method,<sup>17-19</sup> which can be traced back to the early work in the multi-configuration self-consistent field (MCSCF) optimization, provided a decent solution to dynamically adjust the level shift of Hessian eigenvalues. In the state far from the quadratic region, AH works close to the gradient descent method. When the gradients approach to zero, AH equation turns to the normal Newton's equation.

Based on the AH method, we present in this paper a second order optimization algorithm, co-iterative augmented Hessian (CIAH) method for orbital optimization problem. The basic idea of CIAH algorithm is to embed the optimization procedure into the diagonalization procedure of AH equation. The structure of orbital optimization parameters are considered in the algorithm. Particularly, small step is preferred by this algorithm than one shot "optimal" step. The details are described in Section II. This algorithm is universal for a wide range of orbital optimization problem, from Hartree-Fock and Kohn-Sham energy minimization for restricted and unrestricted, closed and open shell, molecule and crystal, to MCSCF optimization and orbital localization. Since MCSCF

<sup>a)</sup>Electronic mail: osirpt.sun@gmail.com

energy minimization is beyond the pure orbital optimization, the relevant algorithm details and convergence performance are documented in our MCSCF work.<sup>20</sup> In Section III, we numerically verified the performance of the algorithm with various kinds of SCF calculations and orbital localization.

## II. ALGORITHM

Provided  $E$  the energy functional of the one-particle orbital rotation  $U$  subjected to the exponential ansatz of the unitary transformation

$$U = e^{\hat{R}}, \quad (1)$$

$$\hat{R} = \sum_{pq} R_{pq} a_p^\dagger a_q, \quad (2)$$

$$R_{pq} = -R_{qp}^*, \quad (3)$$

energy minimization can be treated as a non-linear search problem for the optimized  $\mathbf{R}^*$  where the stationary condition holds

$$\left. \frac{\partial E}{\partial R_{pq}} \right|_{\mathbf{R}^*} = 0.$$

For  $k$ th iteration, a displacement  $\mathbf{x}^{(k+1)}$  to approach the solution  $\mathbf{R}^*$  can be obtained by solving the AH matrix equation

$$\begin{pmatrix} 0 & \mathbf{g}^{(k)\dagger} \\ \mathbf{g}^{(k)} & \mathbf{H}^{(k)} \end{pmatrix} \begin{pmatrix} 1 \\ \lambda \mathbf{x}^{(k+1)} \end{pmatrix} = \epsilon \begin{pmatrix} 1 \\ \lambda \mathbf{x}^{(k+1)} \end{pmatrix}, \quad (4)$$

$$g_{pq}^{(k)} = \left. \frac{\partial E}{\partial R_{pq}} \right|_{\mathbf{R}^{(k)}}$$

$$H_{pq,rs}^{(k)} = \left. \frac{\partial^2 E}{\partial R_{pq} \partial R_{rs}} \right|_{\mathbf{R}^{(k)}}.$$

The AH matrix here plays the role to damp the solution of Newton's method

$$\mathbf{g}^{(k)} + \lambda(\mathbf{H}^{(k)} - \epsilon)\mathbf{x}^{(k+1)} = 0 \quad (5)$$

with level shift

$$\epsilon = \lambda \mathbf{g}^{(k)\dagger} \mathbf{x}^{(k+1)}.$$

The level shift parameter circumvents the descending direction problem when the optimizer is around the non-quadratic region. When the answer approaches the local minimum, Eq. (5) turns to the standard Newton's equation because  $\epsilon$  rapidly decays to zero. The scaling factor  $\lambda$  is commonly used in AH algorithm to adjust the step size.<sup>19,21</sup>

In the CIAH program, we don't have sophisticated step size adjustment. A special feature of orbital optimization is that the matrix elements of the unitary transformation (2) must lie in the range  $[-1, 1]$ . This allows us to fill the optimal rotation matrix with a series of small displacements. Therefore, we simply removed the  $\lambda$  parameter in Eq (4) and scaled down the largest element of the displacement vector  $\mathbf{x}$  to a small predefined threshold  $\delta$

$$\begin{cases} \mathbf{x}^{(k)} & \max(\mathbf{x}^{(k)}) < \delta \\ \frac{\delta}{\max(\mathbf{x}^{(k)})} \mathbf{x}^{(k)} & \text{otherwise} \end{cases}. \quad (6)$$

The thresholds are slightly different in different optimization problems. For SCF and MCSCF wavefunction, we prefer smaller step size  $\delta = 0.03$  to provide a smooth convergence procedure because we usually have reasonable initial guess. In the orbital localization problem, the initial guess is often very different to the final answer. Optimization often starts with canonical orbitals and ends up with local orbitals. A slightly larger threshold  $\delta = 0.05$  is used so that the optimizer can move quickly in the parameter space. Nonetheless, it should be noted that small step generally has advantage over large step in CIAH algorithm.

Because of the small step strategy, it can be expected that the Hessian matrix in the adjacent iterations should be close to each other. Approximately, one can keep the Hessian matrix unchanged and update only the gradients during the optimization iterations. This requires small modification to the Davidson diagonalization program<sup>22</sup> which is used to solve the AH equation (5). In the conventional AH algorithm, one expands and diagonalizes the  $(n+1)$ -rank AH matrix in the subspace representation. In the modified version, we only keep track of the subspace corresponding to the  $n$ -rank Hessian matrix. When the system moved to the new point, we construct the gradients representation with the old  $n$ -rank basis  $\{v\}$  and obtain the new representation of AH matrix

$$\begin{aligned} H_{ij}^{(k+1)} &= \langle v_i^{(k)} | H[\mathbf{R}^{(s)}] | v_j^{(k)} \rangle, \quad s < k, \\ g_i^{(k+1)} &= \langle v_i^{(k)} | g[\mathbf{R}^{(k+1)}] \rangle. \end{aligned}$$

Besides the Hessian reservation treatment, we embedded the function optimization iteration into the Davidson diagonalization iteration. Within each cycle of CIAH updating, the AH diagonalization program enlarges the subspace by one basis vector  $\mathbf{v}$  in terms of the Davidson preconditioner

$$\mathbf{v}^{(k+1)} = (\mathbf{H}_0 - \epsilon)^{-1} (\mathbf{H}\mathbf{x}^{(k)} - \epsilon\mathbf{x}^{(k)}). \quad (7)$$

The Hessian matrix representation is therefore improved gradually during the CIAH optimization cycles. Due to the error in the diagonalization solver, the displacement vector  $\mathbf{x}$  might not be optimal in the early stage of the optimization. The error can be removed in the later steps and the optimal displacement will be generated when the AH diagonalization solver gets enough bases to accurately represent the gradients and the Hessian matrix. The small step strategy plays an important role in the CIAH algorithm because it reduces the negative effects of the poor displacement vector appeared in the early optimization stage.

When the system is around the non-quadratic region, the main purpose of the orbital Hessian is to adjust the direction of the displacement. The accuracy of the Hessian matrix is not highly important in this circumstance. One can take coarse approximations for the orbital Hessian to reduce the computational costs, eg projecting the Hessian from low level basis sets, or superposition of the fragment Hessian matrices. Integral approximations such as density fitting, high cutoff, sparse meshgrids (for DFT numeric integration), or even single precision integrals can be used as well.

Unlike the Hessian approximations, it is less flexible to approximate the orbital gradients. Orbital gradients provide two

aspects of usage: the convergence criteria and a rough optimization direction. The gradients must be accurately evaluated when it was used as the convergence criteria. For the optimization direction, approximated orbital gradients are acceptable. The Taylor expansion of orbital gradients around given point  $\mathbf{R}^{(k)}$  is

$$g[\mathbf{R}] = g[\mathbf{R}^{(k)}] + H[\mathbf{R}^{(k)}] \cdot (\mathbf{R} - \mathbf{R}^{(k)}) + \dots \quad (8)$$

If the new point  $\mathbf{R}$  is close to the expansion point, the gradients at  $\mathbf{R}$  can be approximated by the first order expansion. It should be noted that the first order approximation may cause large error in orbital gradients, especially when approximated Hessian matrix is employed. Our solution is to insert keyframes which are the exact gradients in certain iterations (while the Hessian matrix is still approximated). A keyframe is triggered by two conditions: (i) if the gradients are out of trust region with respect to the previous keyframe, (ii) if the number of iterations between two keyframes is more than the predefined keyframe intervals. The keyframe here provides not only the adjustment to the optimization path, but also a reference to check whether convergence criteria are met.

Here we briefly summarized the CIAH algorithm (Table I is an example of the evolution of each quantities during the optimization procedure).

1. Given an initial value  $\mathbf{R}^{(0)}$ , the optimizer starts to build the AH equation with one trial vector and the AH matrix is a  $2 \times 2$  matrix. Diagonalizing the AH matrix provides the first displacement  $\mathbf{x}^{(0)}$  which is then scaled down to the predefined step-size threshold as shown by Eq. (6).
2. For  $k$ th iteration, the displacement  $\mathbf{x}^{(k)}$  is used to update the Davidson subspace basis  $\mathbf{v}^{(k+1)}$  using Eq. (7) and the gradients  $\mathbf{g}^{(k+1)}$  with the first order approximation (8). The new basis and the approximated gradients are used to build the new AH matrix for the next displacement  $\mathbf{x}^{(k+1)}$ . This step is applied many times until the number of iterations reaches predefined upper limit (go to step 4) or the keyframe is triggered (go to step 3).
3. In the keyframe ( $\mathbf{g}^{(4)}$ ,  $\mathbf{g}^{(7)}$  in Table I), gradients are evaluated exactly based on the cumulated displacements ( $\mathbf{R}^{(0)} + \mathbf{x}^{(1)} + \dots + \mathbf{x}^{(k)}$ ). Based on the exact gradients, there are three different conditions for the program flow: (i) If the norm of gradients is smaller than the required convergence criterion, we will call other convergence checks and prepare to finish the optimization; (ii) if the gradients are very different to the last approximate gradients (out of trust region, in which the ratio between the new and old gradients' norms is over 3), the optimizer will move to step 4; (iii) otherwise, we insert the exact gradients into the AH equation (4) to generate a better displacement vector then go back to step 2.
4. We move the system to the new point ( $\mathbf{R}^{(1)}$  in Table I), then discard all bases of the Davidson diagonalization solver and rebuild the AH matrix (as step 1 did). The last displacement is used as the initial guess of the Davidson diagonalization solver. The program will go

back to step 2 and start a new cycle of optimization. We labelled such a cycle from step 2 - step 4 as a macro iteration.

The number of iterations (micro iterations) within each macro iteration is around 10 in our implementation. In the SCF procedure, the matrix-vector product of the Davidson diagonalization algorithm are the most time-consuming operations. It involves the contraction of J/K (Coulomb and exchange) matrices which is as expensive as the regular Fock matrix construction. The number of J/K contractions in CIAH algorithm is equal to the total number of micro iterations (due to the matrix-vector operations in the AH matrix diagonalization) plus the number of keyframes. By using the Hessian approximations, the real cost can be much lower than that the number of J/K contractions indicated because the time-consuming J/K contractions are restricted in the keyframes. In the CIAH algorithm, small step size is the guarantee for the Hessian and the gradients approximations. These approximations might lead to more macro iterations but generally it reduces the cost of J/K operations thus improves the overall performance.

### III. NUMERICAL ASSESSMENT

The CIAH algorithm were implemented in the open-source electronic structure program package PySCF.<sup>23</sup> In all SCF calculations, the convergence criteria are set to  $10^{-10} E_h$  for the change of energy and  $10^{-5}$  for the norm of gradients. For spatial and spin symmetry, symmetry broken is allowed if it can decrease the total energy. The initial guess orbitals for CIAH solver are fed from the regular DIIS-SCF iterations, of which the change of SCF energy converges to  $1.0 E_h$ . The DIIS-SCF calculations are initialized with the superposition of atomic density. In the DIIS-SCF iterations, unless otherwise specified, DIIS subspace size is 8 and level shift is 0.2. For ROHF methods, DIIS extrapolation is applied on Roothaan's open-shell Fock matrix. The structures of all molecules can be found in the support material.

#### A. Hessian approximations

We use the triplet states of  $\text{Cr}_2$  and Fe-porphine with ROHF/cc-pVDZ and UB3LYP/cc-pVDZ calculations to inspect the HF and DFT Hessian approximations, including density-fitting (DF), basis projection, and sparse grids (for DFT). In the DF approximation, we employed Weigend Coulomb-fit basis as the auxiliary fitting basis which is inaccurate for exchange integrals. In the sparse grids approximation, we computed the second order derivative of XC functionals with small mesh grids in which the number of radial grids and angular grids are (15,86) for light elements and (30,110) for transition metal while the normal mesh grids are (75,302)/(90,434). In the basis projection approximation, we expand the Hessian matrix on single-zeta basis then transform back to cc-pVDZ basis. The single-zeta basis is derived from

TABLE I. The evolution of gradients and Hessians during the CIAH iterations

Macro iter	AH subspace size	Hessians	Gradient	Displacement
1	1	$\mathbf{H}^{(0)} = \frac{\partial^2 E}{\partial \mathbf{R} \partial \mathbf{R}^T} [\mathbf{R}^{(0)}]$	$\mathbf{g}^{(0)} = \frac{\partial E}{\partial \mathbf{R}} [\mathbf{R}^{(0)}]$	$\mathbf{x}^{(1)}$
	2	$\mathbf{H}^{(0)}$	$\mathbf{g}^{(1)} \approx \mathbf{g}^{(0)} + \mathbf{H}^{(0)} \mathbf{x}^{(1)}$	$\mathbf{x}^{(2)}$
	3	$\mathbf{H}^{(0)}$	$\mathbf{g}^{(2)} \approx \mathbf{g}^{(1)} + \mathbf{H}^{(0)} \mathbf{x}^{(2)}$	$\mathbf{x}^{(3)}$
	4	$\mathbf{H}^{(0)}$	$\mathbf{g}^{(3)} = \frac{\partial E}{\partial \mathbf{R}} [(\mathbf{R}^{(0)} + \mathbf{x}^{(1)} + \dots + \mathbf{x}^{(3)})]$	$\mathbf{x}^{(4)}$
	5	$\mathbf{H}^{(0)}$	$\mathbf{g}^{(4)} \approx \mathbf{g}^{(3)} + \mathbf{H}^{(0)} \mathbf{x}^{(4)}$	$\mathbf{x}^{(5)}$
	6	$\mathbf{H}^{(0)}$	$\mathbf{g}^{(5)} \approx \mathbf{g}^{(4)} + \mathbf{H}^{(0)} \mathbf{x}^{(5)}$	$\mathbf{x}^{(6)}$
	7	$\mathbf{H}^{(0)}$	$\mathbf{g}^{(6)} = \frac{\partial E}{\partial \mathbf{R}} [(\mathbf{R}^{(0)} + \mathbf{x}^{(1)} + \dots + \mathbf{x}^{(6)})]$	$\mathbf{x}^{(7)}$
	8	$\mathbf{H}^{(0)}$	$\mathbf{g}^{(7)} \approx \mathbf{g}^{(6)} + \mathbf{H}^{(0)} \mathbf{x}^{(7)}$	$\mathbf{x}^{(8)}$
$\mathbf{R}^{(1)} = \mathbf{R}^{(0)} + \mathbf{x}^{(1)} + \dots + \mathbf{x}^{(8)}$				
2	1	$\mathbf{H}^{(1)} = \frac{\partial^2 E}{\partial \mathbf{R} \partial \mathbf{R}^T} [\mathbf{R}^{(1)}]$	$\mathbf{g}^{(8)} = \frac{\partial E}{\partial \mathbf{R}} [\mathbf{R}^{(1)}]$	$\mathbf{x}^{(9)}$
	2	$\mathbf{H}^{(1)}$	$\mathbf{g}^{(9)} \approx \mathbf{g}^{(8)} + \mathbf{H}^{(1)} \mathbf{x}^{(9)}$	$\mathbf{x}^{(10)}$

TABLE II. Number of macro iterations and key-frames and J/Ks required for different CIAH approximations in  ${}^3\text{Cr}_2$  and  ${}^3\text{Fe-porphine}$  SCF optimization.

		${}^3\text{Cr}_2$			${}^3\text{Fe-porphine}$		
		Macro iters	keyframes	J/Ks	Macro iters	keyframes	J/Ks
ROHF	Standard CIAH	18	51	304	3	8	30
	DF Hessians	19	51	308	3	8	30
	Projected basis	18	37	184	14	24	63
	All in one	14	33	159	14	24	63
UB3LYP	Standard CIAH	17	38	150	9	21	84
	DF Hessians	17	39	170	10	21	87
	sparse grids	19	41	157	9	20	85
	DF +sparse grids	17	39	153	9	20	85
	Projected basis	26	49	183	22	39	147
	All in one	25	47	164	22	39	147

cc-pVDZ basis by removing the outermost one shell for each angular momentum. The single-zeta basis significantly reduces the number of basis functions, from 86 to 54 for  $\text{Cr}_2$  and from 439 to 159 for Fe-porphine. Level shift is not applied in the initial guess of  ${}^3\text{Cr}_2$  because level shift leads to a symmetry reserved solution which is high in total energy.

In Figure 1, we compare the SCF convergence for standard CIAH (without applying above approximations) and the approximate CIAH iterations. The convergence curves of DF Hessian and sparse grids are close to the standard CIAH curve in all tests, presenting that they have high quality approximations to the Hessian matrix. The basis projection approximation has large error because it misses large fraction of the Hessian matrix. Except the early stage of the optimization, such error leads to obvious deviation to the standard CIAH convergence curve. In three of the tests, this poor approximation can converge the SCF to the right answer but require two times of the macro iterations or more. For  ${}^3\text{Cr}_2$  ROHF, there are several local minimum answers. Depending on the numerical fluctuation during the optimization, basis projection can occasionally converge to the lowest one.

Table II shows the number of macro iterations, key-frames and J/K contractions for each Hessian approximations. In the standard CIAH procedure, the costs to compute key-frame are roughly equal to the costs of J/K contraction. The total costs

are determined by the number of J/K contractions which are the dominant operations in the Hessian construction. In the approximate schemes, the Hessian construction becomes less expensive. The computational dominant step turns to the key-frame construction. For schemes like DF and sparse grids, the number of key-frames is around 25% of the number of J/K contractions. One could get 2 - 3 times speed up for the overall performance. For example, by using the density fitting for  ${}^3\text{Fe-porphine}$  UHF Hessian, the Hessian construction takes only 25% of the total computing time while it needs over 70% of the computing time in the standard CIAH treatment. In practice, even the poor basis projection approximation has significant performance advantage over the standard CIAH iteration since it requires much less keyframes than the number of J/K contractions of the standard CIAH scheme.

## B. CIAH vs. DIIS

Based on the tests of Hessian approximations, the combination of DF and sparse grids provides an efficient scheme to approximate the Hessian matrix without the penalty of the convergence rates. They are adopted in our following SCF calculations. Applying basis projection at early optimization stage can further improve the total computing costs. This treatment

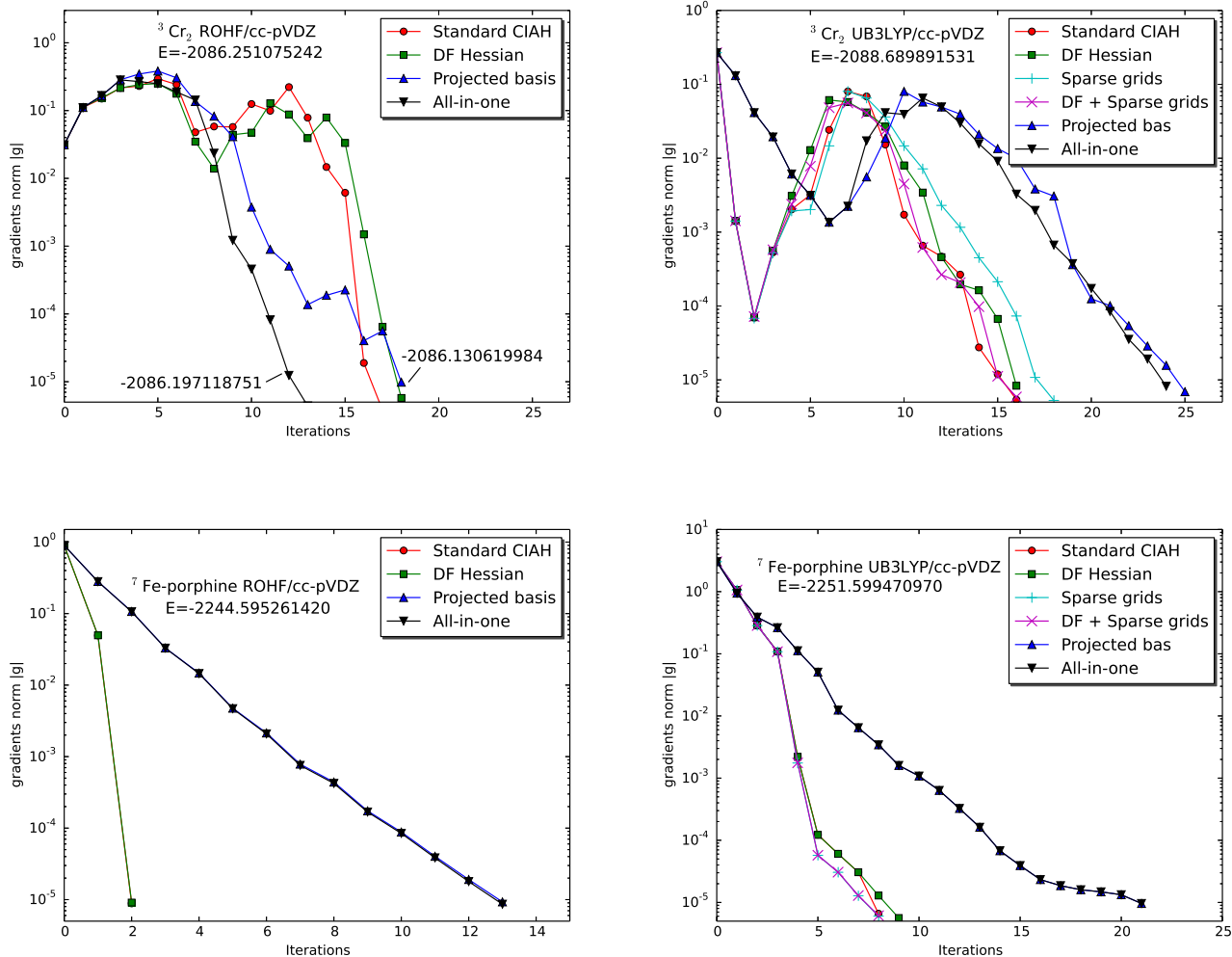


FIG. 1. SCF convergence for different Hessian approximations.

is not applied in the comparison because it is largely associated with the initial guess than optimization iterations.

Table III presents the results of CIAH and DIIS for some challenging SCF systems. The CIAH algorithm shows better overall convergence than the DIIS algorithm. Except  ${}^3\text{UF}_4$  with U-LSDA/LANL2DZ, CIAH is able to converge all test systems. Using DIIS, 5 systems do not meet the convergence criteria within 500 SCF iterations. For the converged systems, there are 8 answers that CIAH and DIIS algorithms show good agreements. Aside from the 8 systems, CIAH and DIIS predicts closed solutions in 3 systems:  ${}^3\text{Cr}_2$  with U-LSDA/3-21G,  ${}^1\text{UF}_4$  with B3LYP/LANL2DZ and  ${}^3\text{UF}_4$  with U-B3LYP/LANL2DZ. In the 3 systems, CIAH solution is about  $1 mE_h$  (or less) lower than DIIS solution. For the rest systems (except  ${}^3\text{UF}_4$  with U-LSDA which is not converged in CIAH), noticeable differences can be found between the two algorithms: the total energy predicted by CIAH algorithm is lower. Most of these systems are associated to the

unrestricted calculations. These CIAH solutions have larger spin-contamination than that appeared in DIIS solutions. In these systems, spin-symmetry broken happens on the early stage of CIAH iterations which is not observed in the entire DIIS iterations. One possibility is the side effect of DIIS level shift. Although level shift stabilizes the DIIS oscillations, it limits the variational space that the optimization solver can reach. Some DIIS solutions actually converge to the saddle point. For example, feeding the DIIS solution of  ${}^3\text{UF}_4$  with UHF/LANL2DZ to the CIAH solver, CIAH takes 7 extra iterations to move to the expected lower-energy answer  $E = -448.736476864$ .

### C. Orbital localization

CIAH algorithm can be applied with various type of orbital localization methods. Here we only demonstrated the

TABLE III. CIAH vs. DIIS. Level shift 0.2 is applied in DIIS. For the unconverged solutions, the values are reported up to (without) the oscillated decimal place.

Molecule	Method	CIAH <sup>e</sup>	$E$	DIIS	$E$
<sup>1</sup> Cr <sub>2</sub> <sup>a</sup>	LSDA/3-21G	18 (40)	-2073.907478426	191	-2073.907480839
	B3LYP/3-21G	5 (11)	-2078.075421673	31	-2078.075421674
<sup>3</sup> Cr <sub>2</sub> <sup>a</sup>	U-LSDA/3-21G	55 (175)	-2073.949040592	328	-2073.948413591
	U-B3LYP/3-21G	75 (135)	-2078.244163328	56	-2078.175189832
<sup>1</sup> UF <sub>4</sub> <sup>a</sup>	LSDA/LANL2DZ	15 (38)	-448.6767448225	184	-448.6767448158
	B3LYP/LANL2DZ	23 (56)	-451.0320849544	> 500	-451.03129955
<sup>3</sup> UF <sub>4</sub> <sup>a</sup>	ROHF/LANL2DZ	18 (53)	-448.7341401101	431	-448.7176513294
	UHF/LANL2DZ	8 (27)	-448.7364768642	424	-448.7203771973
	U-LSDA/LANL2DZ	> 500	-448.7307	193	-448.7310709215
	U-B3LYP/LANL2DZ	130 (188)	-451.0971319546	132	-451.0970715829
<sup>1</sup> Ru <sub>4</sub> CO <sup>b</sup>	RHF/LANL2DZ	13 (34)	-484.6768737985	125	-484.6768611861
	B3LYP/LANL2DZ	8 (19)	-488.4169663521	99	-488.4169663513
<sup>3</sup> Ru <sub>4</sub> CO <sup>b</sup>	ROHF/LANL2DZ	12 (30)	-484.7310915959	> 500	-484.675
	UHF/LANL2DZ	29 (82)	-484.9692302601	> 500	-484.6947
	U-B3LYP/LANL2DZ	123 (211)	-488.4555228944	280	-488.4348633206
<sup>3</sup> Fe-porphine <sup>c</sup>	ROHF/cc-pVDZ	3 (8)	-2244.597443185	22	-2244.597443185
	UHF/cc-pVDZ	5 (14)	-2244.708766895	> 500	-2244.6360
	U-B3LYP/cc-pVDZ	9 (20)	-2251.599470970	32	-2251.599470969
<sup>1</sup> Fe <sub>4</sub> S <sub>8</sub> C <sub>4</sub> H <sub>12</sub> <sup>-d</sup>	RHF/cc-pVDZ	18 (44)	-8387.977176947	> 500	-8387.7108
	B3LYP/cc-pVDZ	8 (21)	-8399.568031935	165	-8399.568031918

<sup>a</sup> Geometry is taken from Ref<sup>14</sup>

<sup>b</sup> Geometry is taken from Ref<sup>6</sup>

<sup>c</sup> Geometry is taken from Ref<sup>24</sup>

<sup>d</sup> Geometry is taken from Ref<sup>25</sup>

<sup>e</sup> Number in parenthesis is the total keyframes

convergence of Boys localization (see Figure 2) for the HF occupied orbitals and virtual orbitals of buckyball at RHF/cc-pVTZ level as an example. Although not presented in this paper, Edmiston-Ruedenberg and Pipek-Mezey localization can be accelerated by the same solver.

Unlike the SCF initial guess, orbital localization often starts with canonical orbitals, which is typically very different to the final answer. For buckyball, the canonical orbitals cannot be directly taken as the initial guess for Boys localization because the orbital gradients are strictly zero (at saddle point). One solution is to add small noise on the initial guess to drive the system out of the saddle point. This is marked as “random” in Figure 2. Another initial guess we tried is pre-localization which is marked as “atomic” in Figure 2. In the atomic initial guess, we compare the canonical orbitals  $\psi$  with a set of reference atomic orbitals  $\chi$  to define the rotation  $\tilde{U}$  in terms of the SVD of the projection  $\langle \chi | \psi \rangle$

$$\begin{aligned} \langle \chi | \psi \rangle &= U \lambda V^\dagger, \\ \tilde{U} &= V U^\dagger. \end{aligned}$$

Transformation  $\tilde{U}$  thus defines the initial guess orbitals  $|\tilde{U}\psi\rangle$  which are close to the reference atomic orbitals.

For occupied orbitals, the two kinds of initial guess produce small difference on the optimization procedure and converge to the same solution. The random initial guess is slightly worse at beginning. After about 7 steps to move out of the sad-

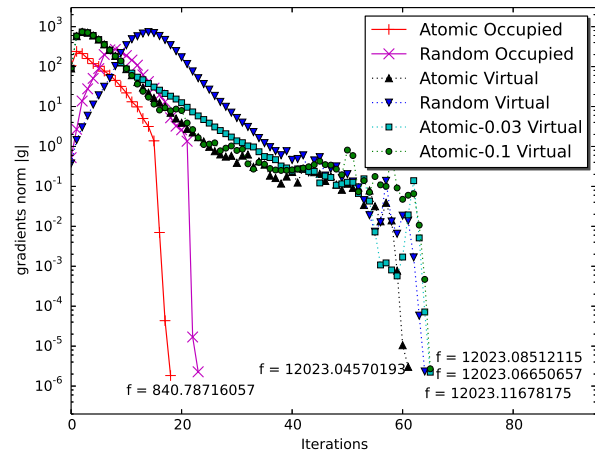


FIG. 2. Boys localization for C<sub>60</sub> molecule. The object function is  $f = \sum_i \langle ii | (\mathbf{r}_1 - \mathbf{r}_2)^2 | ii \rangle$ .

dle point, it shows the similar convergence curve as the atomic initial guess. The orbital localization becomes difficult when diffused orbitals are involved. There are many local minimum solutions close to each other. For buckyball virtual orbitals, different initial guess (atomic and random), different step size

(0.03, 0.05, 0.1) lead to different solutions in which the values of object function are differed by 0.05 au or around. Regard to the system size and the total value of object function (12023 au), the difference is negligible.

Since the initial guess is so different to the answer, one may expect that the large step size is superior. In fact, the tests for the three step size (0.03, 0.05 and 0.1) have closed convergence performances. They all take around 30 iterations to move away from the initial guess and the next 30 iterations wandering around the quadratic region. Once the solver steps into the quadratic region, they rapidly converge to the solution. Although not obvious in the figure, we observed during the optimization that the step size 0.1 sometimes overshoots the displacement and causes oscillation on the object function value. This observation numerically supports that the small step size is able to provide better gradients and Hessian estimations than the large step size.

#### IV. CONCLUSION

In this work, we demonstrated a general second order algorithm CIAH for orbital optimization problem. In the CIAH algorithm, the optimization is embedded in the augmented Hessian diagonalization procedure. The evaluation of gradients and Hessian matrix are decoupled. Various approximations can be used for the Hessian matrix. By analyzing and comparing three Hessian approximations: density fitting, sparse grids, basis projection, we find that the combination of density fitting and sparse grids is able to produce high quality approximations to the Hessian matrix. Our numerical tests of SCF convergence suggests that CIAH is a stable, reliable and efficient algorithm for SCF energy minimization problem. Apart from the molecular SCF energy minimization, CIAH algorithm can be used in many orbital optimization scenarios, such as orbital localization, MCSCF orbital optimization, SCF energy minimization with periodic boundary condition. Our numerical tests of orbital localization verifies the capability of CIAH algorithm to localize a large number of diffuse orbitals.

CIAH algorithm offers a new possible solution for a wide range of optimization problem. To make CIAH general purpose optimization algorithm, some problems remain for further study. First is the constraint optimization. In the orbital optimization, the normalization constraints are imposed indi-

rectly by the exponential ansatz for the unitary transformation. Applying the normalization constraints in a direct manner can avoid the expensive matrix exponential operation, which is particularly useful for large scale systems. Moreover, the constraint optimization would extend CIAH to the area of geometry optimization and the transition state search. Second is the step size for a general purpose optimization problem since the small step assumption might not work efficiently in the general parameter space.

#### V. ACKNOWLEDGMENTS

This work was supported by the National Science Foundation through NSF-CHE-1657286.

- <sup>1</sup>P. Pulay, *Chem. Phys. Lett.* **73**, 393 (1980).
- <sup>2</sup>P. Pulay, *J. Comput. Chem.* **3**, 556 (1982).
- <sup>3</sup>E. Cancès and C. Le Bris, *Int. J. Quantum Chem.* **79**, 82 (2000).
- <sup>4</sup>V. R. Saunders and I. H. Hillier, *Int. J. Quantum Chem.* **7**, 699 (1973).
- <sup>5</sup>K. N. Kudin, G. E. Scuseria, and E. Cancès, *J. Chem. Phys.* **116**, 8255 (2002).
- <sup>6</sup>X. Hu and W. Yang, *J. Chem. Phys.* **132**, 054109 (2010), <http://dx.doi.org/10.1063/1.330499>.
- <sup>7</sup>E. Cancès, *J. Chem. Phys.* **114**, 10616 (2001).
- <sup>8</sup>L. Thøgersen, J. Olsen, D. Yeager, P. Jørgensen, P. Salek, and T. Helgaker, *J. Chem. Phys.* **121**, 16 (2004).
- <sup>9</sup>L. Thøgersen, J. Olsen, A. Köhn, P. Jørgensen, P. Salek, and T. Helgaker, *J. Chem. Phys.* **123**, 074103 (2005), <http://dx.doi.org/10.1063/1.1989311>.
- <sup>10</sup>S. Høst, J. Olsen, B. Jansík, L. Thøgersen, P. Jørgensen, and T. Helgaker, *J. Chem. Phys.* **129**, 124106 (2008), <http://dx.doi.org/10.1063/1.2974099>.
- <sup>11</sup>S. Host, B. Jansik, J. Olsen, P. Jørgensen, S. Reine, and T. Helgaker, *Phys. Chem. Chem. Phys.* **10**, 5344 (2008).
- <sup>12</sup>Y. A. Wang, C. Y. Yam, Y. K. Chen, and G. Chen, *J. Chem. Phys.* **134**, 241103 (2011), <http://dx.doi.org/10.1063/1.3609242>.
- <sup>13</sup>Y. K. Chen and Y. A. Wang, *J. Chem. Theory Comput.* **7**, 3045 (2011).
- <sup>14</sup>A. D. Daniels and G. E. Scuseria, *Phys. Chem. Chem. Phys.* **2**, 2173 (2000).
- <sup>15</sup>T. H. Fischer and J. Almlöf, *J. Phys. Chem.* **96**, 9768 (1992).
- <sup>16</sup>F. Neese, *Chem. Phys. Lett.* **325**, 93 (2000).
- <sup>17</sup>B. H. Lengsfeld, *J. Chem. Phys.* **73**, 382 (1980).
- <sup>18</sup>P. Jørgensen, P. Swannstrom, and D. L. Yeager, *J. Chem. Phys.* **78**, 347 (1983).
- <sup>19</sup>H.-J. A. Jensen and P. Jørgensen, *J. Chem. Phys.* **80**, 1204 (1984).
- <sup>20</sup>Q. Sun and G. K.-L. Chan, *Chem. Phys. Lett.* (2017), submitted.
- <sup>21</sup>D. Ghosh, J. Hachmann, T. Yanai, and G. K.-L. Chan, *J. Chem. Phys.* **128**, 144117 (2008), <http://dx.doi.org/10.1063/1.2883976>.
- <sup>22</sup>E. R. Davidson, *J. Comput. Phys.* **17**, 87 (1975).
- <sup>23</sup>Q. Sun, "Python module for quantum chemistry program," <https://github.com/sunqm/pyscf.git> (2014).
- <sup>24</sup>A. R. Groenhof, M. Swart, A. W. Ehlers, and K. Lammertsma, *J. Phys. Chem. A* **109**, 3411 (2005).
- <sup>25</sup>S. Sharma, K. Sivalingam, F. Neese, and C. Kin-Lic, *Nat. Chem.* **6**, 927 (2014).